Systematic investigation of cracks in encapsulated solar cells after mechanical loading

Martin Sander[a,*], Sascha Dietrich[a], Matthias Pander[a], Matthias Ebert[a], Jörg Bagdahn[a,b]

[a]*Fraunhofer Center for Silicon Photovoltaics, Walter-Hülse-Str. 1, 06120 Halle (Saale), Germany*
[b]*Anhalt University of Applied Sciences, Photovoltaic Materials, Bernburger Str. 57, 06366 Köthen (Anhalt), Germany*

Abstract

Mechanical and thermal loads on photovoltaic modules (PV modules) lead to mechanical stresses in the module parts and especially in the encapsulated solar cells which can break under a certain load. To investigate the development of cracks in encapsulated solar cells a novel approach was developed that systematically analyzes the influence of the load direction on the crack directions. For this purpose an experiment is established that tests specimens on smaller scales under well-known boundary conditions. The cell cracks are statistically evaluated and the fracture stress can be compared directly for different crack orientations or different cell types. The test setup is expected to be suitable to systematically investigate the behavior of new cell or module designs or to act as a quality assurance test.
For the investigated cells a loading parallel to the busbars causes cracks at lower load magnitudes than a loading perpendicular to the busbars and different cell types show different fracture strength values. The findings can be transferred to full scale modules by calculating a probability of failure for each solar cell. This allows an interpretation of many effects that were observed in full scale modules and allows design optimization for reduced cell breakage rates.

Keywords:
cracks, electroluminescence, mechanical loading, thermal loading

1. Introduction

Photovoltaic modules (PV modules) are supposed to have a lifetime of more than 20 years under various environmental conditions like temperature changes, wind load, snow load, etc. Such loads induce mechanical stresses into the components of the module, especially into the crystalline solar cells, which show cracks frequently [1–3]. The cracks are mostly invisible for optical inspection (naked eye) but can be identified using electroluminescence [4]. Thus they are often called micro-cracks even though their dimension is on millimeter or even centimeter scale [5, 6]. The cracks can lead to isolated cell areas, thus causing reduced power output of the module [5, 6].
According to IEC 61215 full scale PV modules are tested mechanically by applying a uniform

*Corresponding author: Tel.: +49 345 5589 416; FAX: +49 345 5589 101
Email address: martin.sander@csp.fraunhofer.de (Martin Sander)

area load on the horizontally mounted PV module. Typically after this mechanical load test the cells of the PV modules show a characteristic crack pattern that corresponds with observations on PV modules in the field, too. These characteristic crack directions can be found for both mono-crystalline and multi-crystalline cells [7].
The crack orientation in the cells and the spatial distribution of cracks in the module varies over the cell position [7]. This indicates a non-uniform stress distribution and different stress directions in individual cells in the PV module under mechanical loading. To analyze this in more detail some preliminary mechanical considerations on the stress distribution in full scale PV modules are discussed in Section 2.
To get more information about the mechanics of crack development and crack growth in encapsulated solar cells, tests of mini-modules under well-known boundary conditions are performed. The loading conditions are derived from the stress analysis in full scale PV modules.
The experimental approach and the test setup is described in Section 3. Cracks after mechanical loading are investigated systematically and different types are identified in Section 4. They are evaluated according to their relative frequency of occurrence in PV modules and the fracture stress for different cell types is determined. These results can be transferred to full scale PV modules by using finite element analysis (FEA). Using this approach adjustments in module mounting or module design can be made to reduce cell cracks and to increase module reliability.

2. Stress conditions in full scale PV modules

The strain and stress distribution of the cross section of a PV laminate is depicted schematically in Fig. 1a for a uniaxial bending around the y axis. Compression stress at the top side of the glass and tension stress at the bottom side is induced in x-direction. The cells are placed at the bottom side of the module. Thus tension strain from the bottom side of the glass is transferred to the cells via the encapsulant. The material properties of the encapsulant have an influence on the transferred stress into the cells. This stress is superimposed with the bending stress of the cell itself. The highest tension stress occurs at the bottom side of the cells leading to breakage of the silicon as shown by Dietrich et al. [8].
To analyze the stress distribution in full scale PV modules under a uniform area load, a finite element simulation has been set up that includes all relevant materials and layers. Due to the symmetry a simulation of a quarter of the module with appropriate boundary conditions meets the requirements. Figure 1b shows the first principal stress at the bottom side of the cells of a standard PV module with an aluminum frame which is clamped with four clamps at the long edges. Additionally, the representative direction for the first and the second principal stress for each cell is depicted by arrows. The arrow size represents the stress magnitude. With these information the characteristic crack pattern of PV modules after mechanical load test can be explained well in a qualitative way. Despite the large variety of crack orientations classified by Köntges et al. [9], in the following it is assumed that the crack orientations can be condensed to cracks parallel, perpendicular and 45° to the busbars, because all other classes are found to be combinations of these.
It is obvious that most of the cells show a biaxial stress distribution and the first and second principal stresses are aligned predominantly in x- and y-direction. Here cracks either parallel or perpendicular to the busbars can be observed, in which cracks parallel to the busbars may lead to isolated areas and therefore to power loss of the PV module [7, 9]. In particular the four cells in the corners of the module show a 45° stress direction and the highest stress magnitude. This is the position where most of the PV modules show cracks under 45° after mechanical loading [7].

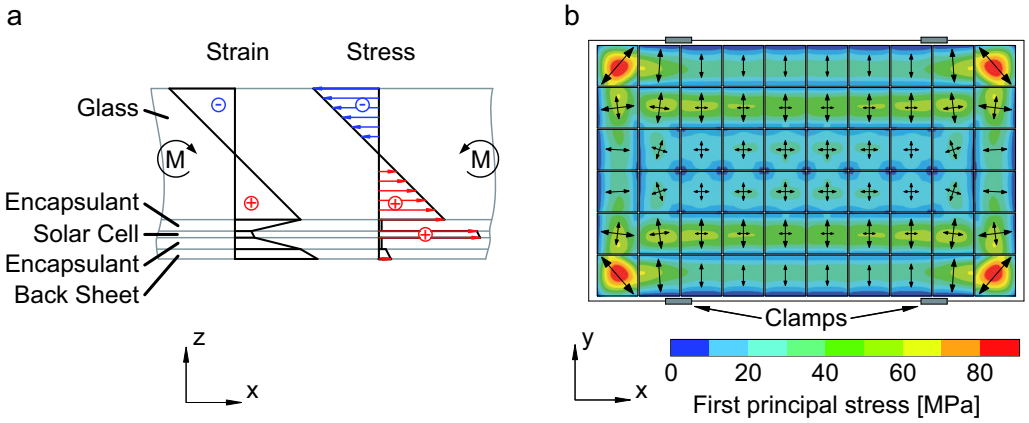

Figure 1: (a) Schematic strain and stress distribution for a PV laminate during bending around the y-axis [8]. (b) Standard PV module with a clamped aluminum frame under 5.4 kPa area load. The color code represents the magnitude of the first principal stress at the bottom side of the cells and the representative direction for the first and the second principal stress is depicted by arrows.

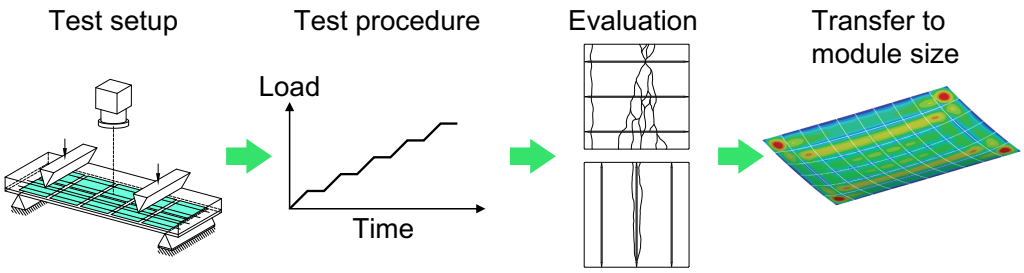

Figure 2: Experimental approach for investigation of directional mechanical loading.

The non-uniform stress distribution and different stress directions make it difficult to estimate the fracture stress for an individual cell or to set up a reliability concept for the cells in a PV module just by performing standard mechanical load tests on module scale.

3. Experimental approach

To achieve an improvement in mechanical characterization of encapsulated solar cells a new experimental approach is chosen that investigates cracks systematically according to their direction. For first investigations the influence of stresses in x- and y-direction is analyzed. Figure 2 shows schematically the experimental approach for investigation of mechanical loading. For this purpose test specimens on smaller scales (mini-modules) are exposed to defined loads and are characterized by electroluminescence.

3.1. Test specimens

In previous publications test specimens with hand soldered solar cells were investigated [2, 10]. In this work industrially soldered cell strings with either multi-crystalline or mono-

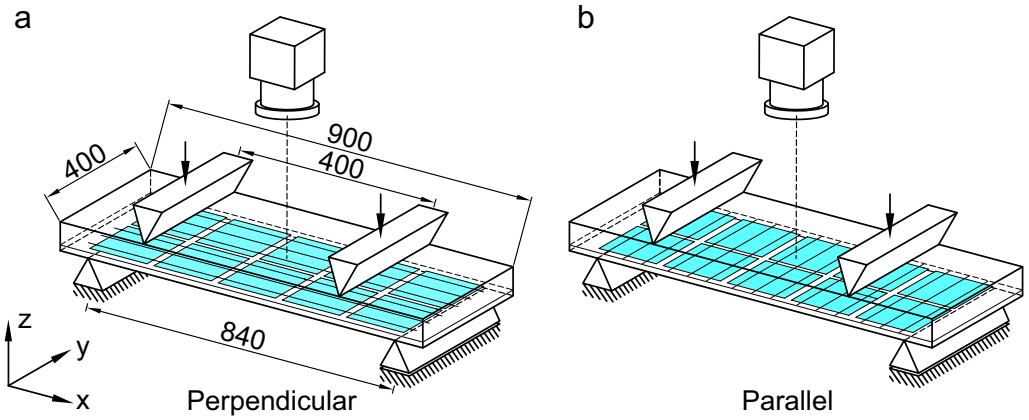

Figure 3: Schematic test setup for the investigation of the effect of mechanical loading; (a) Bending perpendicular to the busbars; (b) Bending parallel to the busbars.

crystalline cells were used. Figure 3 shows schematically the layout of the test specimens. The mini-modules consist of 10 solar cells, a 4 mm full tempered glass pane, an EVA encapsulant and a polymeric backsheet. The cells have standard dimensions (156 mm x 156 mm x 180 µm). In the first step multi-crystalline and mono-crystalline cells were compared. The mini-modules are laminated using laboratory equipment. Therefore, the process parameters are selected preferably similar to the industrial processes. By using equal cells, the influence of varied specimen layouts or process parameters on the fracture behavior can be investigated.

3.2. Test setup

Figure 3 shows the schematic test setup for mechanical loading. The test specimens are supported by two rolls at their bottom side and are loaded by two rolls on their top side. If the specimen consists of cells that have their busbars perpendicular to the load rolls, the setup is called perpendicular (Fig. 3a) and if the busbars of the cells are parallel to the load rolls, the setup is called parallel (Fig. 3b).

The experimental setup represents a 4-point bending setup, for which the stress distribution can be calculated analytically for a monolithic beam or plate [11].

For a layered test specimen with several solar cells, the stress distribution is not uniform because of the separated solar cells and the transformed tension stress from the glass bottom side as described in Section 2. To analyze the strain in the test specimens, the finite element model of the full scale module (see Section 2) is used and adapted to the dimensions of the specimen. An assessment of the simulation results proves that during mechanical loading stress is induced predominantly in x-direction in the test specimen. The distance between the support rolls and between the load rolls was adjusted to approximate an equal stress field for the three cell pairs in the middle of the test specimen (see Fig. 4a). Furthermore, the stress field in one cell is insignificantly affected by a crack in an adjacent cell (see Fig. 4b). So crack occurrences in all six cells in the field of view of one test specimen can be analyzed under equal conditions.

The area of the specimen between the two load rolls is inspected using an electroluminescence camera (Sensovation coolSamBa HR-830). The bending setup is mounted on a universal testing machine (Zwick Z400). The load rolls are driven by the crosshead of the machine. The load

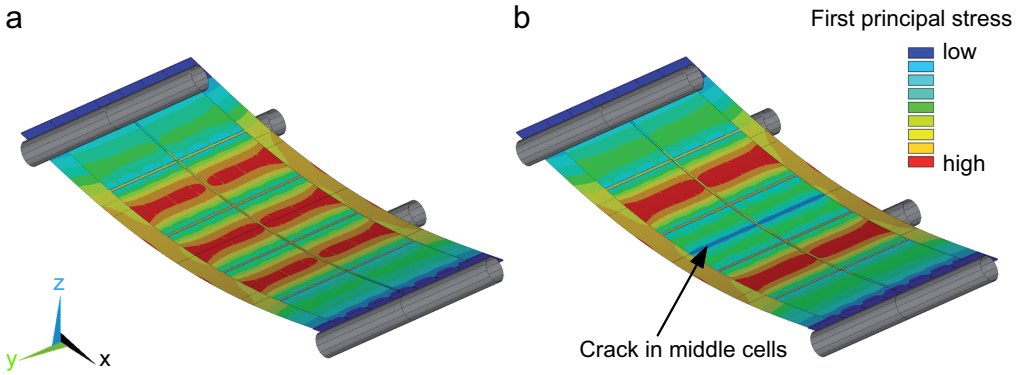

Figure 4: First principal stress at bottom side of silicon and glass in a test specimen during 4-point bending; (a) with intact cells; (b) with completely broken middle cells.

is measured by a load cell (maximum load 10 kN) between the load rolls and the machine crosshead. The deflection of the middle of the test specimen is measured by a displacement sensor (maximum displacement 100 mm) that is mounted on the frame of the machine. The camera is mounted on the machine crosshead in order to move together with the load rolls. So the focus of the camera stays constant during the test procedure. The field of view of the camera was adjusted to inspect the six cells between the load rolls.

3.3. Test conditions and test procedure

All tests were performed at room temperature. The test specimens were analyzed after each manufacturing step and after defined load steps using qualitative electroluminescence imaging. The load is increased stepwise and remains applied for a short time (60 s) while the EL image is taken. At the end of the test procedure a load time curve and EL images for every load step are available. Figure 5 shows exemplarily a measurement curve of a test specimen. In the diagram in Fig. 5a the load steps are visible on the time scale. The load over displacement plot (Fig. 5b) illustrates the approximately linear behavior of the load test. The simulated displacement of the specimen is plotted as well and indicates that the simulation represents the experiment very well. At high load magnitudes one can identify crack occurrences when the load decreases abruptly. This cracking produces also a perceivable acoustic noise. The stiffness of the specimen is decreased slightly by a cracked cell. The load is increased until all cells in the field of view are broken or a previously defined maximum load is reached.

3.4. Evaluation

The EL images are evaluated manually. Reliable crack identification and assessment is possible if images are compared before and after loading. If a crack propagates, its origin can be identified and analyzed in the previous steps.
If a crack is observed in the EL image for the first time at a specific load step, the force at which this crack occurs is determined from the load time data (see Fig. 5). The crack origin is identified from the EL image, which corresponds to the load step. With these two information the fracture stress is calculated using results from the finite element analysis (see Fig. 4). The

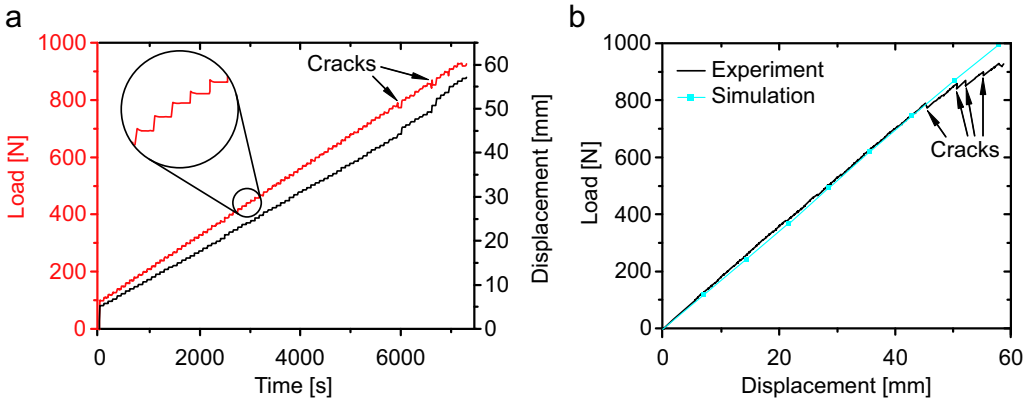

Figure 5: (a) Measured load (red) and displacement (black) curve over time of a test specimen with crystalline cells and (b) measured and simulated load over displacement curve for the same test specimen.

calculated fracture stress represents the occurrence of one crack. The influence of the cracking of an adjacent cell is also considered (see Fig. 4b). So from one test specimen up to six crack occurrences can be obtained and six fracture stress values can be calculated.

Because of the brittle material characteristic of silicon at room temperature, the fracture stress values show a large scatter. In order to evaluate the observed fracture characteristic in terms of strength one has to deal with the mechanical behavior of this type of material. Brittle materials do not show a yield strength and plastic deformation, thus they cannot compensate excessive stress with any kind of ductility. As a results fracture occurs suddenly and catastrophic under tensile load [12]. The origin of the fracture is one particular defect such as microscopic cracks, inclusions or dislocations with a critical size. The size as well as the location of those defects is statistically distributed. As a consequence the macroscopic fracture stress follows this distribution and leads to a large scatter of strength values for each specimen. Because of this scatter a comprehensive statistical evaluation of the stress values has to be carried out. Typically the Weibull distribution function [13] is used for silicon although other distribution functions might be suitable as well. Two characteristic parameters are determined by a Weibull evaluation, the characteristic strength σ_θ and the Weibull modulus m as a measure for the scattering. The probability of failure P_f represents the probability that a specimen breaks at a specific stress σ. The characteristic strength σ_θ represents the stress for a probability of failure of 63.2 %. If the Weibull modulus m is higher, the scattering of the fracture stress values is lower, indicating higher reliability at equal strength.

$$P_f(\sigma) = 1 - e^{-\left(\frac{\sigma}{\sigma_\theta}\right)^m} \tag{1}$$

As a result of the randomly distributed defects the characteristic strength depends on the size of the component, because in a larger area the probability of having a bigger defect is higher and therefore the characteristic strength is lower for a bigger size of the component. This dependency is called the size effect [13].

In this work the size effect is not considered explicitly. This simplification is assumed to be acceptable for this work, because the behavior of cracks shall be analyzed qualitatively.

If an adequate number of occurrences of cracks is available, the characteristic fracture strength σ_θ and the Weibull modulus m can be calculated.

4. Results and Discussion

4.1. Cracks after mechanical loading

Figure 6 shows the EL images of four specimens with mono-crystalline and multi-crystalline cells during mechanical loading at different load steps.

It was found that some cells in the unloaded specimens show partially small cracks after soldering or after lamination. These cracks were mainly observable at the beginning or at the end of the busbars. They are estimated to be caused by thermal or mechanical loading during production. Starting from these existing cracks new cracks occurred during mechanical loading at relative low load values. The cracks beginning from existing cracks show a different behavior than cracks without a visible existing crack at their origin, because their paths are often unbranched and seldom dendritic.

Examples for both types are shown in Fig. 6. In the specimen with multi-crystalline cells in the perpendicular layout the cell at the right in the top row shows a crack beginning at a pre-existing crack at the bottom busbar (at 210 N). The other cracked cells show dendritic crack paths indicating higher energy release [7].

The EL images for mono-crystalline cells show cracks at higher load magnitudes which run mostly under 45° to the cell edges. This is characteristic for mono-crystalline cells, because here cracks propagate along the <110> sliding plane that is oriented under 45° to the cell edges [12]. Furthermore, it was observed that if cracks start from pre-existing cracks at lower load magnitudes, they propagate not exact under 45°. These cracks showed partially a stepwise crack propagation at successive load increase.

Based on these findings it was decided to separate between cracks starting at existing cracks, called damaged state, and cracks without visible existing cracks, called undamaged state.

The crack occurrences were evaluated and fracture stress values were calculated as described in Section 3.4. All fracture stress values were evaluated using a Weibull distribution function. The Weibull plot is displayed in Figure 7 for all test specimens. It includes data from four specimens with mono-crystalline and four specimens with multi-crystalline cells. Two of each four specimens were loaded parallel to the busbars and two specimens were loaded perpendicular. The determined Weibull parameters are listed in Table 1.

The undamaged mono-crystalline cells show the highest fracture stress values and the characteristic strength is higher for the perpendicular layout.

The undamaged multi-crystalline cells loaded perpendicular to the busbars show only slightly lower fracture stress values, but if they are loaded parallel to the busbars, the fracture stress values are significantly lower.

The curves for the damaged state (open symbols) show lower characteristic strengths than the curves for the undamaged state (filled symbols). This indicates that if a cell has an existing crack of a visible size, it will fail under low stress magnitudes. Additionally, the loading parallel is more critical than the loading perpendicular to the busbars. The plot and the Weibull distribution values show the basic differences between the two classes damaged and undamaged, but do not contain information about their relative frequency. To gain information about the percentage of cells which have existing cracks after production, the EL images of all specimens were analyzed after production with respect to existing cracks (see Section 4.2).

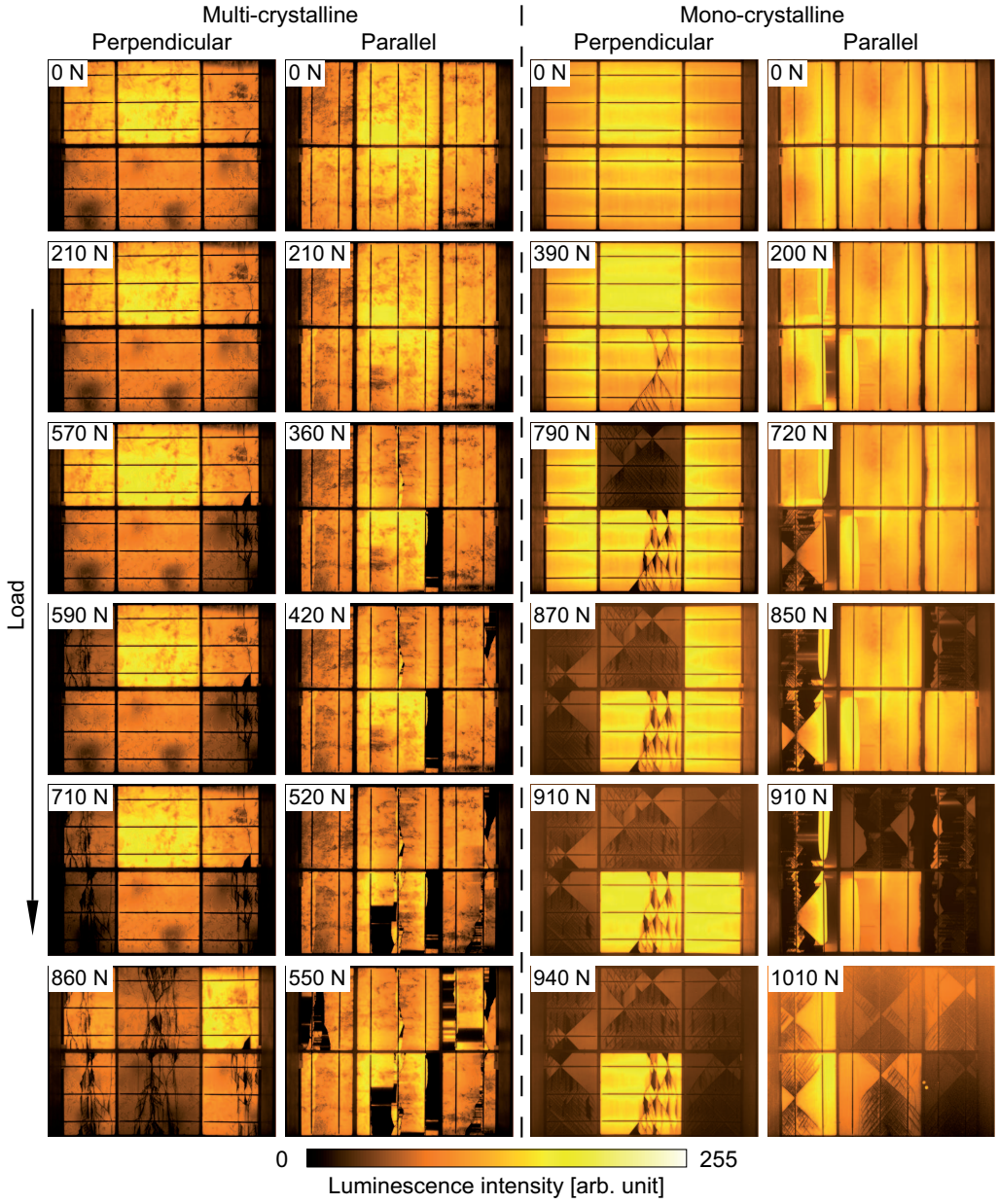

Figure 6: Electroluminescence image of the middle cells of test specimens with multi-crystalline and mono-crystalline cells during 4-point bending at different load steps (displayed in false color representation).

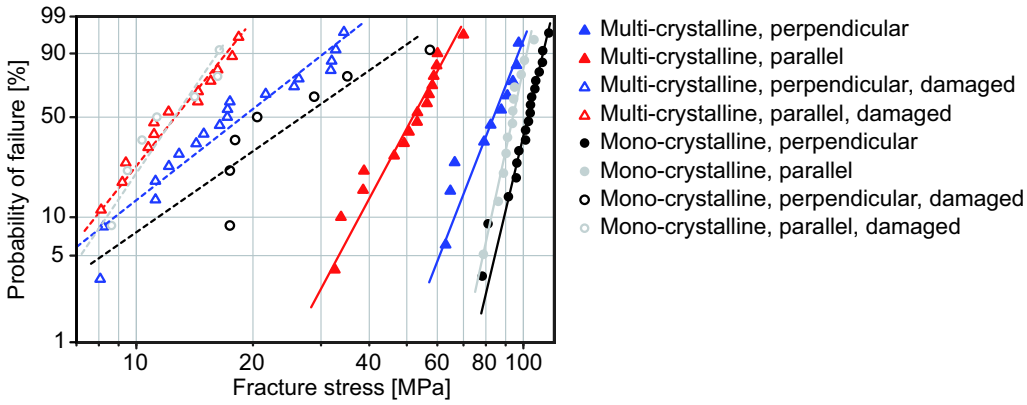

Figure 7: Weibull plot of crack occurrences in test specimens with mono-crystalline and multi-crystalline cells.

	σ_θ MPa	m -
Multi-crystalline, parallel	55.2 (50.1...60.4)	5.9 (3.8...8.4)
Multi-crystalline, perpendicular	87.6 (79.7...95.5)	8.1 (4.6...13.1)
Multi-crystalline, parallel, damaged	13.8 (11.8...16.0)	4.0 (2.5...5.8)
Multi-crystalline, perpendicular, damaged	21.8 (17.7...26.5)	2.5 (1.7...3.4)
Mono-crystalline, parallel	96.4 (92.2...100.6)	14.7 (9.1...21.3)
Mono-crystalline, perpendicular	105.7 (101.6...109.7)	13.3 (8.8...18.7)
Mono-crystalline, parallel, damaged	13.6 (11.1...16.4)	4.7 (2.4...7.9)
Mono-crystalline, perpendicular, damaged	30.3 (21.5...41.7)	2.3 (1.4...3.5)

Table 1: Investigated Weibull distribution values according to Fig. 7, (values for 95 % confidence interval in brackets)

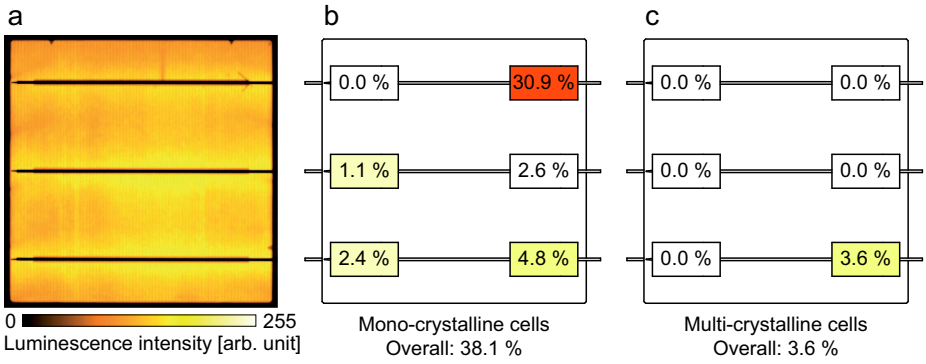

Figure 8: a) Electroluminescence image of a representative mono-crystalline cell in a test specimen after lamination; b, c) Percentage of observed cracks at possible crack origin positions for all test specimens after lamination.

4.2. Cracks after production

Figure 8 shows a detail of a representative test specimen with mono-crystalline cells, which show several visible cracks originating mainly at the busbars. A statistical evaluation of the cracks with respect to their origin allows conclusions about an increased incidence of cracks at certain positions and therefore about critical loading during manufacturing.

Most of the cracks occurred after lamination at the side where the interconnector runs from the front side of one cell to the back side of the next cell. Here the soldered string with the individual cells has to withstand the mechanical pressure and the different expansion of the individual components during temperature change from lamination temperature to room temperature.

For example the investigated mono-crystalline cells in Fig. 8b showed a higher number of cracks at the top busbar on the right hand side. This might be caused by an inhomogeneous soldering process. The overall percentage of cells that show minimum one crack after soldering for this specimen type is 38.1 %. For the tested multi-crystalline cells a percentage of 3.6 % for minimum one visible crack was observed. Here only visible cracks in the EL images are considered, but there might be more that are smaller or that are placed under the solder ribbon.

4.3. Transfer to module layout

In the 4-point bending test the cells are bent uniaxially. The stress distribution in a framed and clamped PV module is more complex, but can be analyzed by finite element analysis. If the simulated stress distribution in the PV module is evaluated with the statistically determined fracture strength values, a fracture probability per cell can be calculated for specific cell fracture strengths. In this work a simplified approach for calculating the probability of failure is chosen that does not consider the size effect (see Section 3.4).

Figure 9 shows the procedure for calculating the probability of failure per cell. The cells in the corners of the module are excluded, because no fracture strength values for 45° twisted cells were investigated, yet. The used fracture strength values correspond to multi-crystalline cells (see Figure 9b and Table 1). The probability of failure is calculated independently for x- (blue) and y-direction (red) for each cell based on the maximum stress magnitude in the silicon for the individual cells (Fig. 9c and d). For brittle materials like silicon it is assumed that the

stresses σ_x and σ_y can cause a fracture of a cell independently from each other (principle of independent action) [14]. So the probability of fracture per cell $P_{f,cell}$ is calculated by multiplying the individual probabilities of survival in x- and y-direction (Fig. 9e).

$$P_{f,cell} = 1 - e^{-\left(\frac{\sigma_{x,max}}{\sigma_{\theta,x}}\right)^{m_x} - \left(\frac{\sigma_{y,max}}{\sigma_{\theta,y}}\right)^{m_y}} \tag{2}$$

Due to the lower fracture strength values in y-direction the failure probability is dominated by the cracks parallel to the busbars (Fig. 9c). The only cells that are prone to break perpendicular to the busbars are the cells at the short edge of the module (Fig. 9d).
For this module layout and the investigated multi-crystalline cells one would expect that with a probability of 99.6 % at least one cell will show a crack after a mechanical load test with an area load of 5.4 kPa, if no cell would have an existing crack after lamination.
The probability of failure of a module that contains only damaged cells is calculated by using the values for damaged cells. For the applied area load of 5.4 kPa the probability of failure is very high for nearly all the cells in the module (not shown here). So, if cells have existing cracks, they will break with a high probability at loads that are below 5.4 kPa. To estimate the total probability of failure, the probability of failure for the damaged cells is weighted by multiplying it by the percentage P_{Damage} of cells that showed visible cracks after production (Fig. 9f, 3.6 % for multi-crystalline cells; see Section 4.2), wihich means that 3.6 % of the cells in the module have an existing crack after production, regardless their position in the PV module.

$$P_{f,cell,damaged} = P_{Damage} \cdot \left(1 - e^{-\left(\frac{\sigma}{\sigma_{\theta,damaged}}\right)^{m_{damaged}}}\right) \tag{3}$$

The probability of failure for a module that contains damaged and undamaged cells is then calculated by multiplying the individual probabilities of survival for the damaged and undamaged cells (Fig. 9g). This plot homogenizes the probability of failure, because a damaged cell will fail with a high probability, but there is a certain probability that any cell contains an existing crack. The overall probability of having at least one cracked cell in a PV module that contains damaged and undamaged cells after mechanical load test with an area load of 5.4 kPa is expected to 99.8 %.

The calculated values are in a similar range as the observed fracture probabilities in experiments [7, 9], but cannot be compared absolutely because the cell properties and the boundary conditions of the experiment are not known.

5. Conclusion and Outlook

This work shows a novel approach to investigate crack formation and crack growth in encapsulated solar cells systematically. By using the experimental setup influences of mechanical loading can be analyzed under well-known boundary conditions and the observed mechanisms can be transferred to full scale PV modules using a simplified evaluation method.
A test setup that creates a uniaxial bending of the test specimens was used for systematical investigation of the influence of stress on the crack direction. The solar cells were tested parallel and perpendicular to their busbars because these two load cases are dominant in standard PV modules. It was found that loading parallel to the busbars is more critical than perpendicular especially for multi-crystalline cells and that cracks occur preferentially at existing cracks from

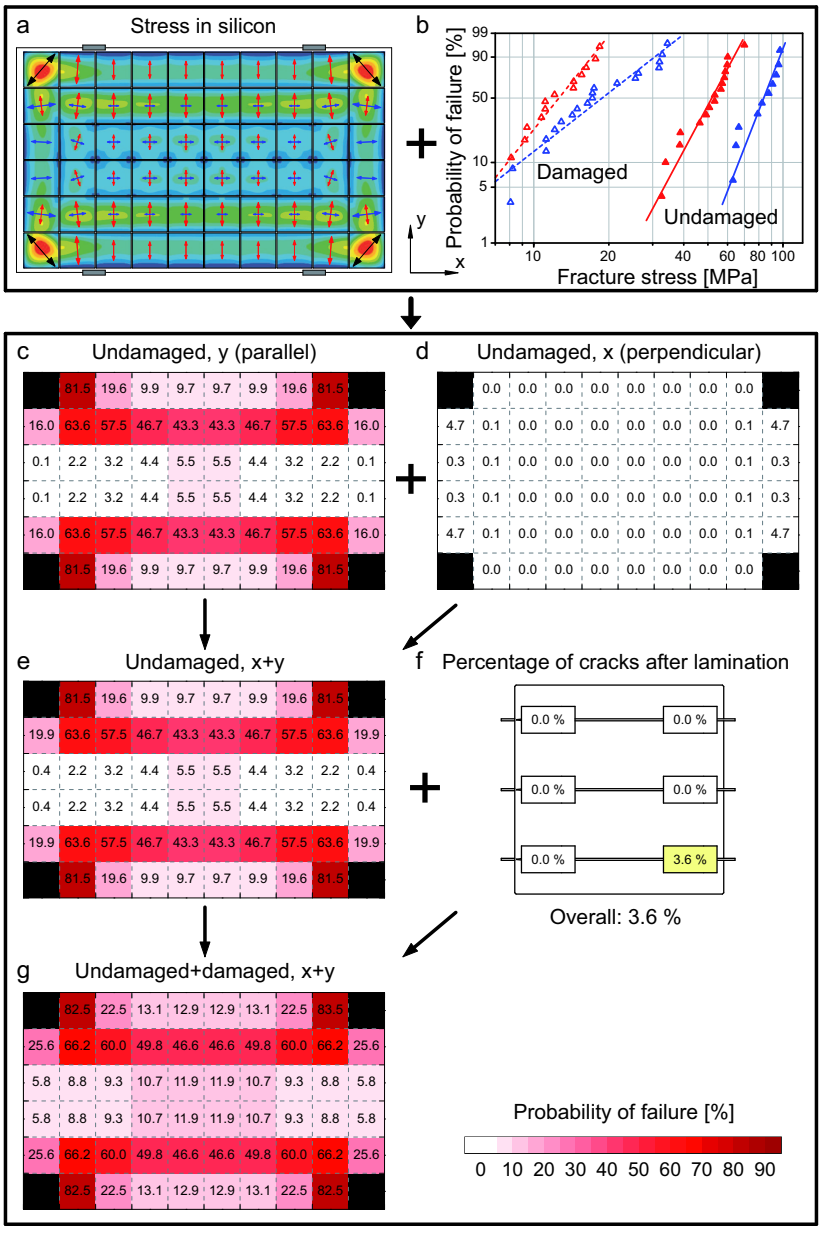

Figure 9: Procedure for calculating the probability of failure per cell for a standard PV module with a clamped aluminum frame under 5.4 kPa area load. The Weibull parameters refer to multi-crystalline cells (corners excluded).

the soldering or lamination process. The fracture strength was evaluated statistically so that a probability of failure per cell can be derived for full scale PV modules by using finite element analysis. The findings correlate well with statistical data from the field [7, 9].
The conclusions allow an interpretation of many effects that were observed in full scale PV modules and show possibilities for optimization approaches. Cracks that are induced by the production process of the PV module should be avoided as far as possible, because they act as starting points for crack growth at low stress magnitudes. It might be promising to influence the direction of the first principal stress inside the cells in that way that it is aligned with the direction of the busbars of the cells, because in this direction higher fracture strength values have been found. This can be done, for example, by changing the mounting of the module [14]. Additionally, the stress magnitude can be influenced by changing the layout of the module [14].
Furthermore, the presented experimental setup can be used to compare different cells or varied process parameters like soldering or lamination temperature or pressure to find out their influences on the fracture strength of the encapsulated cells. Using this approach helpful information can be generated with reasonable time and effort and can be used to estimate the probability of failure in the full size PV module.

Acknowledgments

This work was supported by the Federal Ministry for Education and Research (BMBF) within the InnoProfile project ”SiThinSolar” (project no. 03IP607) and the ”Spitzencluster Solarvalley” project ”xμ-Module” (project no. 03SF0400A) that is gratefully acknowledged. In addition, the authors would like to thank the group Optical Materials and Spectroscopy at Fraunhofer CSP for their support on the test equipment, the team Polymeric Materials at Fraunhofer CSP for their support during specimen lamination and Frank Wenger and Sascha Lindig for their support in specimen preparation and execution of the tests.

References

[1] A. Gabor, M. Ralli, S. Montminy, L. Alegria, C. Bordonaro, J. Woods, J. Felton, Soldering induced damage to thin Si solar cells and detection of cracked cells in modules, in: Proceedings of the 21st European Photovoltaic Solar Energy Conference (2006), pp. 2042–2047.

[2] M. Sander, S. Dietrich, M. Pander, S. Schweizer, M. Ebert, J. Bagdahn, Investigations on crack development and crack growth in embedded solar cells, in: Proceedings of SPIE –The International Society for Optical Engineering, vol. 8112 (2011), pp. 811209-1-811209-10.

[3] M. Sander, B. Henke, S. Schweizer, S. Dietrich, M. Pander, M. Ebert, J. Bagdahn, Systematische Untersuchung der Rissentstehung und des Rissfortschritts in eingebetteten Solarzellen, in: Proceedings of the 26th Symposium Photovoltaische Solarenergie (2011), pp. 302 – 307.

[4] T. Fuyuki, H. Kondo, T. Yamazaki, Y. Takahashi, Y. Uraoka, Photographic surveying of minority carrier diffusion length in polycrystalline silicon solar cells by electroluminescence, Applied Physics Letters 86 (2005), pp. 1–3.

[5] P. Grunow, P. Clemens, V. Hoffmann, B. Litzenburger, L. Podlowski, Influence of micro cracks in multi-crystalline silicon solar cells on the reliability of PV modules, in: Proceedings of the 20th EUPVSEC (2005), pp. 2042–2047.

[6] M. Köntges, I. Kunze, S. Kajari-Schröder, X. Breitenmoser, B. Bjørneklett, The risk of power loss in crystalline silicon based photovoltaic modules due to micro-cracks, Solar Energy Materials and Solar Cells 95 (2011), pp. 1131 – 1137.

[7] S. Kajari-Schröder, I. Kunze, U. Eitner, M. Köntges, Spatial and orientational distribution of cracks in crystalline photovoltaic modules generated by mechanical load tests, Solar Energy Materials and Solar Cells 95 (2011), pp. 3054 – 3059.

[8] S. Dietrich, M. Pander, M. Sander, S.H. Schulze, M. Ebert, Mechanical and thermo-mechanical assessment of encapsulated solar cells by finite-element-simulation, in: Proceedings of SPIE - The International Society for Optical Engineering vol. 7773 (2010), pp. 77730F-1 – 77730F-10.

[9] M. Köntges, S. Kajari-Schröder, I. Kunze, U. Jahn, Crack statistic of crystalline silicon photovoltaic modules, in: Proceedings of the 26th European Conference on Photovoltaic Solar Energy (2011) , pp. 3290–3294.
[10] M. Sander, B. Henke, H. Schwarz, S. Dietrich, S. Schweizer, M. Ebert, J. Bagdahn, Characterization of PV modules by combining results of mechanical and electrical analysis methods, in: Proceedings of SPIE - The International Society for Optical Engineering vol. 7773 (2010), pp. 777308-1 – 777308-12.
[11] Standard, DIN EN ISO 1288-3: Determination of the bending strength of glass - Part 3: Test with specimen support at two points (four point bending), 2007.
[12] S. G. Roberts, Fracture and brittle-ductile transition in silicon, in: R. Hull (Ed.), Properties of crystalline silicon, INSPEC, The Institution of Electrical Engineers, London, United Kingdom, pp. 144–148.
[13] Standard, ASTM 1239-07: Reporting uniaxial strength data and estimating weibull distribution parameters for advanced ceramics, 2007.
[14] S. Dietrich, M. Sander, M. Pander, M. Ebert, Interdependency of mechanical failure rate of encapsulated solar cells and module design parameters, in: Proceedings of SPIE - The International Society for Optical Engineering vol. 8472 (2012), pp. 84720P-1 – 84720P-10.